Desalination and Water Treatment
www.deswater.com

doi: 10.5004/dwt.2023.29430

291 (2023) 214–223
April

Online real-time control of hydroturbine regulation system fault with state time lag

Lin Cui[a], Meng Li[a], Jie Ding[a], Fang Fang[a], Mengyao Lu[a], Sheng Wu[b,*]

[a]*National Ocean Technology Centre, Tianjin 300112, China*
[b]*Yantai Research Institute, Harbin Engineering University, Harbin 150001, China, email: wusheng@hrbeu.edu.cn*

Received 29 April 2022; Accepted 21 July 2022

ABSTRACT

Mechanical faults, time-varying faults and other disturbances in the role of multiple coupling, the stable operation of the hydroturbine regulation system has caused great obstacles. This study concentrated on the output feedback fault-tolerant (FFT) control technology and T-S state feedback predictive control technology using the actual operating conditions of the numerical simulation test. The results show that the control technique has good identification tracking and control effect, and can make the system stabilize within 2 s in the case of disturbance. This shows that the control system designed by the research institute has good applicability and provides data reference for the intelligent control operation and maintenance of the hydroturbine regulation system.

Keywords: Hydroturbine; Regulation system; Fault diagnosis; Fault-tolerant control

1. Introduction

In the intelligent control system of hydropower plant, the hydroturbine regulation system is one of the core equipment, which integrates electrical, hydraulic and mechanical with high-dimensional nonlinear characteristics and multiple input and output characteristics [1]. In the operating conditions, the hydroturbine regulation system has a variety of complex operating conditions, such as start-up and shutdown, load shedding, no-load operation [2]. Under the long-term operation under high load conditions and the existence of many inevitable random disturbances, various mechanical failures will inevitably occur in hydroturbine regulation system [3]. The system's ability to operate safely and steadily is significantly hampered by the coupling effect between these flaws and outside disturbances. Intelligent prediction and fault-tolerant governor control can reduce grid frequency fluctuation and preserve the grid's and the hydropower unit's stable operation [4]. In this study, the state time lag and fault disturbance of the regulating system are taken into account to investigate the fault online real-time control of the hydroturbine regulating system, to further enhance the control effect.

1.1. Related works

The hydroturbine regulating system, a vital component of a hydropower plant's intelligent system, has drawn a lot of interest from academics. There have been a lot of studies done on the failure issues with hydroturbines and their regulation systems. Li et al. [5] extended the traditional impact analysis method in analyzing the failure of offshore hydroturbine support structures. The weights of three indicators were reset, including severity, occurrence and detectability. Based on the analysis, improvement and prevention measures are proposed to ensure the safety of the support structure. By comparing with the traditional model, the method is better practical application value and eliminates the limitation of risk priority pole number in the traditional model.

* Corresponding author.

Zhang et al. [6] argued that hydroturbine risk assessment is important for hydroelectric safety of hydro power plants. The traditional algorithm provides poor estimates of vibration range and frequency, so the extended boundaries are optimized by combining path planning. The results show that this method can improve the data fitting performance and facilitate the quantitative and accurate evaluation results. Chen and Tong [7] established a steam hydroturbine regulation system to solve the problem of insufficient stability. The stability categories are obtained by introducing the transfer coefficient characteristics. And the additional momentum approach is used to optimize the multilayer feedforward network algorithm. Results from the test set demonstrate that the technique can precisely distinguish between the hydroturbine stability categories. Zhang et al. [8] described in detail the nonlinear dynamic phenomena such as the stability of hydroturbine balance curve, the position of bifurcation point and the direction of limit cycle, to improve the prediction accuracy of hydroturbine regulation system. The results show that there are multiple complex types of hydroturbine regulation system stability, which provides a way to study the dynamic behavior. Additionally, a guide for parameter setup is provided to guarantee the stability and security of the regulating system. Guo et al. [9] found that the hydroturbine regulating system has a certain pressure pulsation in the tail pipe during operation. In order to examine its impact on the stability of the system, the hydroturbine regulation system dynamics model incorporates the pressure pulsation of the tail pipe. A pressure pulsation damping frequency is proposed to provide a method for stabilizing the regulation system. Ding et al. [10] found that small hydroturbines are less efficient and prone to blockage. Therefore, counter-rotating rotors were used to address these drawbacks. Through pressure fluctuation experiments, the study examined the stability of tiny hydroturbines. The findings indicate that the new model's pressure fluctuation is less extreme, with a maximum reduction of 74.22% between peaks. The feasibility of the new model was verified. Babu et al. [11] found that slurry and air bubble erosion severely damaged the use of the hydroturbine. Therefore, the hydroturbine coating was improved using deep cooling treatment to enhance its resistance to erosion. For comparison, other common hydroturbine coating materials were subjected to erosion resistance experiments together. The results show that the research designed coating has more than 1.5 times higher resistance to slurry erosion and 1.6 times higher resistance to air bubble erosion.

In summary, scholars have carried out optimization studies on the hydroturbine regulation system from various perspectives, such as intelligent algorithms and equipment materials. The aim is to improve the prediction accuracy of its fault occurrence and reduce the occurrence rate of faults. However, at this stage, there are few studies on the online real-time control of the hydroturbine regulation system, which can provide some reference for fault prediction or prevention. In order to provide data support and idea guidance for further increasing the control effect, this study analyzes online real-time control technology while taking the state time lag and fault disturbance of the regulating system into account.

2. Fault-tolerant control technology for hydroturbine regulation system output feedback with state time lag

2.1. System state feedback predictive control technique based on T-S fuzzy model

The Takagi-Sugeno (T-S) fuzzy model can infinitely approximate any smooth nonlinear function, so it has been widely used in solving nonlinear problems [12]. The hydroturbine regulation system has complex nonlinear, stochastic and uncertain problems. The following mathematical model is a general six-dimensional nonlinear hydroturbine regulation system.

$$\begin{cases} \dot{x}(t) = f\left(x(t), u(t)\right) \\ y = \mathbf{C}x(t) \end{cases} \tag{1}$$

When $t \geq 0$, there exists $x(t) \in R^n$, $u(t) \in R^n$; C and y are the output matrix and output value of the system, respectively.

The T-S fuzzy rule in Eq. (2) is applied to build a discrete fuzzy model to transform the nonlinear problem into a linear control problem.

$$\begin{aligned} &\text{IF } x_1(k) \text{ is } M_1^i, x_2(k) \text{ is } M_2^i, \ldots \\ &\text{Then } x(k+1) = \mathbf{A}_i x(k) + \mathbf{B}_i u(k) + \mathbf{Z}_i \end{aligned} \tag{2}$$

where i denotes the i-th fuzzy rule, M denotes the input fuzzy set, $x(k)$ denotes the fuzzy variables; the coefficient matrix and control matrix are denoted by A_i and B_i; $u(k)$ denotes the control vector; Z is the constant vector, and it is usually regarded as the zero vector. Using μ as the affiliation function, the global equation of state of the nonlinear system can be derived. Where, $0 \leq h_i(k) \leq 1, \sum_{i=1}^{i} h_i(k) = 1$.

$$\begin{aligned} x(k+1) &= \sum_{i=1}^{i} h_i(k)\mathbf{A}_i x(k) + \sum_{i=1}^{i} h_i(k)\mathbf{B}_i u(k) \\ h_i(k) &= \frac{\mu_j^i\left(x_j(k)\right)}{\sum_{j=1}^{l} \mu_j^i\left(x_j(k)\right)} \end{aligned} \tag{3}$$

The state feedback prediction control chart of the system is built using the discrete T-S model, as illustrated in Fig. 1 [5]. y denotes the actual system output and $\hat{y}$ denotes the predicted system output. Through feedback correction and rolling optimization, the system can achieve the best predictive control effect.

For the purpose of analysis, the following definitions are made here.

$$\begin{aligned} &H_{j\mathbf{A}} = \sum_{i=1}^{i} h_i(k+1)\mathbf{A}_i, H_{j\mathbf{B}} = \sum_{i=1}^{i} h_i(k+1)\mathbf{B}_i \\ &\mathbf{H}_{(p-1)\mathbf{A}} = \mathbf{H}_{(p-2)\mathbf{A}} = \ldots = \mathbf{H}_{1\mathbf{A}} = \sum_{i=1}^{i} h_j^s \mathbf{A}_i \to \mathbf{A} \\ &\mathbf{H}_{(p-1)\mathbf{B}} = \mathbf{H}_{(p-2)\mathbf{B}} = \ldots = \mathbf{H}_{1\mathbf{B}} = \sum_{i=1}^{i} h_j^s \mathbf{B}_i \to \mathbf{B} \\ &h_i(k+q) = h_i \end{aligned} \tag{4}$$

The overall state equation of the system at the moment of adding the sampling can be expressed by Eq. (5).

$$x(k+p)=\mathbf{A}^{p}x(k)+\sum_{i=1}^{p}\mathbf{A}^{(i-1)}\mathbf{B}u(k-i+p) \tag{5}$$

Therefore, the output prediction for the future sampling moment p_j can be obtained according to Eq. (5).

$$\hat{y}_j(k+p_j)=\mathbf{C}_j\mathbf{A}^{p_j}x(k)+\sum_{i=1}^{p_j}\mathbf{C}_j\mathbf{A}^{(i-1)}\mathbf{B}u(k-i+p_j) \tag{6}$$

Ensuring a consistent time step of the prediction, the current output prediction value can be obtained from the historical input values and the historical state of the system based on Eq. (6). Eq. (7) is the expression of the current output prediction value.

$$\hat{y}_j(k)=\mathbf{C}_j\mathbf{A}^{p_j}x(k-p_j)+\sum_{i=1}^{p_j}\mathbf{C}_j\mathbf{A}^{(i-1)}\mathbf{B}u(k-i) \tag{7}$$

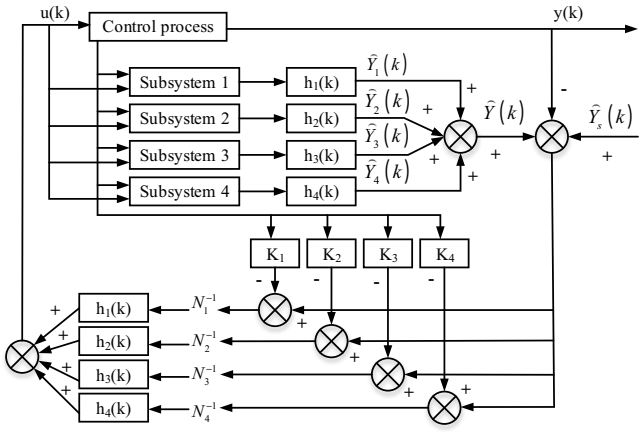

Fig. 1. Diagram of state feedback and predictive control based on the T-S fuzzy model.

Through the feedback correction mechanism, the predicted value of p_j at the future moment is shown in Eq. (8) [13].

$$Y_{cj}(k+p_j)=\hat{y}_j k+\hat{y}_j p_j+y_j(k)-\hat{y}_j(k) \tag{8}$$

2.2. System fault prediction and diagnosis controller model design

x_1, x_2, and x_3 are intermediate state variables; u_1, u_2, and u_3 are three predictive controllers, the mathematical model of hydroturbine predictive control and its parameters are shown in Eq. (9).

$$\begin{cases}\dot{x}_1=x_2\\ \dot{x}_2=x_3\\ \dot{x}_3=-a_0x_1-a_1x_2-a_2x_3+y\\ \dot{\delta}=\omega_0\omega+u_1\\ \dot{\omega}=\dfrac{1}{T_{ab}}\left[m_t-\dfrac{E'_qV_s}{x'_{d\Sigma}}\sin\delta-\dfrac{V_s^2}{2}\dfrac{x'_{d\Sigma}-x'_{q\Sigma}}{x'_{d\Sigma}x'_{q\Sigma}}\sin 2\delta-D\omega\right]+u_2\\ \dot{y}=-\dfrac{1}{T_y}y+\dfrac{1}{T_y}u_3\end{cases} \tag{9}$$

In Eq. (18), $a_0=\dfrac{24}{e_{qh}h_wT_r^3}$, $a_1=\dfrac{24}{T_r^2}$, $a_2=\dfrac{3}{e_{qh}h_wT_r}$, $b_0=\dfrac{24e_y}{e_{qh}h_wT_r^3}$, $b_1=\dfrac{24ee_y}{e_{qh}T_r^2}$, $b_2=\dfrac{3e_y}{e_{qh}h_wT_r}$, $b_3=\dfrac{ee_y}{e_{qh}}$. According to the actual hydraulic control situation, the optimal predictive control parameters are designed, as shown in Table 1 [14].

According to the control parameters designed in Table 1, $a_0=24$, $a_1=24$, $a_2=3$, $b_0=24$, $b_1=-33.6$, $b_2=3$, $b_3=-1.4$.

The feedback matrix is obtained by approximating the system according to the fuzzy rules. If $\delta(t)$ is F_t, then

Table 1
Optimal predictive diagnostic control design parameters taking values

Test parameters	Parameter name	Parameter values	Test parameters	Name	Parameter values
e	Intermediate variables of the receiver	0.65~0.75 p.u.	D	Damping factor	0.45~0.55 p.u.
e_y	Stroke transfer coefficient	0.9~1.1 p.u.	δ	Generator power angle	/
e_{qh}	Head transfer coefficient	0.45~0.55 p.u.	ω_0	Rated angular speed of the generator	320 rad/s
T_{ab}	Mechanical inertia time constant	7.5~8.5 s	V_s	Infinite bus voltage	0.9~1.1 p.u.
T_y	Reaction time constant of the receiver	0.09~0.11 s	$x'_{d\Sigma}$	/	1.14~1.16 p.u.
E'_q	transient potential	1.3~1.4 p.u.	$x'_{q\Sigma}$	/	1.47~1.48 p.u.
h_w	Pressure leadpipe characteristic coefficient	2.0	T_r	Water strike inertia time constant	1.0

$$\begin{cases}\dot{x}(t) == \mathbf{A}_i x(t) + \mathbf{B}_i u(t) \\ y(t) = \mathbf{C}_i x(t)\end{cases}, \text{where } \mathbf{F}_1 = \frac{1}{4}\left(1+\frac{\delta^2}{v^2}\right), \mathbf{F}_2 = \frac{1}{4}\left(1-\frac{\delta^2}{v^2}\right),$$

$$\mathbf{F}_3 = \frac{1}{4}\left(1+\frac{\delta^4}{v^4}\right), \mathbf{F}_4 = \frac{1}{4}\left(1-\frac{\delta^4}{v^4}\right), \ v = 1.6.$$

According to the above analysis, the hydroturbine regulation system can be simplified into four subsystems under the control of four fuzzy rules. The state feedback matrix K_i and reversible matrix N_i^{-1} of the four subsystems can be obtained based on the design parameters of the best predictive diagnostic control.

$$K_1 = \begin{bmatrix} 34.2022 & -4.6939 & 4.0229 & 0.5393 & 52.4755 & -0.3704 \\ 0.8954 & -0.1982 & 0.0969 & -0.0134 & 0.5293 & -0.0047 \\ 0 & 0 & 0 & 0 & 0 & 0.1353 \end{bmatrix}$$

$$N_1^{-1} = \begin{bmatrix} 4.5767 & -157.4012 & -0.3589 \\ 0.0364 & 4.7181 & 0.0777 \\ 0 & 0 & 1.1564 \end{bmatrix} \quad (10)$$

$$K_2 = \begin{bmatrix} 33.9612 & -4.6746 & 3.9971 & 0.5420 & 51.9193 & -0.3675 \\ 0.8850 & -0.1970 & 0.0958 & -0.0133 & 0.5147 & -0.0046 \\ 0 & 0 & 0 & 0 & 0 & 0.1353 \end{bmatrix}$$

$$N_2^{-1} = \begin{bmatrix} 4.5756 & -158.0435 & -0.3598 \\ 0.0367 & 4.7902 & 0.0782 \\ 0 & 0 & 1.1564 \end{bmatrix} \quad (11)$$

$$K_3 = \begin{bmatrix} 34.2309 & -4.6908 & 4.0233 & 0.5393 & 52.5323 & -0.3705 \\ 0.8988 & -0.1985 & 0.0972 & -0.0134 & 0.5334 & -0.0047 \\ 0 & 0 & 0 & 0 & 0 & 0.1353 \end{bmatrix}$$

$$N_3^{-1} = \begin{bmatrix} 4.5769 & -157.1056 & -0.3596 \\ 0.0366 & 4.7311 & 0.0781 \\ 0 & 0 & 1.1564 \end{bmatrix} \quad (12)$$

$$K_4 = \begin{bmatrix} 34.2798 & -4.6974 & 4.0291 & 0.5387 & 52.6087 & -0.3711 \\ 0.8985 & -0.1985 & 0.0972 & -0.0134 & 0.5328 & -0.0047 \\ 0 & 0 & 0 & 0 & 0 & 0.1353 \end{bmatrix}$$

$$N_4^{-1} = \begin{bmatrix} 4.5768 & -157.2653 & -0.1439 \\ 0.0364 & 4.7068 & 0.1730 \\ 0 & 0 & 11.5837 \end{bmatrix} \quad (13)$$

3. Hydroturbine regulation system fault diagnosis and fault-tolerant controller design

3.1. System fault diagnosis and fault-tolerant control techniques with state time lag

In the hydroturbine regulation system, the mechanical hydraulic part is responsible for converting the output signal into the displacement action of the receiver [15]. In this way, the speed and power of the unit can be controlled. The mathematical model of the hydroturbine regulating system includes a delay term to account for the mechanical displacement of the catcher's delay effect. A nonlinear time-delay dynamic mathematical model is obtained, as shown in Eq. (14).

$$\begin{cases}\dot{x}(t) = \mathbf{A}x(t) + \mathbf{B}u(t) + \varphi\left(x(t), x\left(t-\tau(t)\right)\right) + \mathbf{F}_a f_a(t) \\ y(t) = \mathbf{C}(t)\end{cases} \quad (14)$$

where x, u, and y represent the system state vector, input vector, and output vector, respectively. A, B, C, Fa denote the state matrix, input matrix, output matrix and fault matrix, which are constant value matrices of known dimensions [16]. The function $\phi(\cdot)$ is a nonlinear continuous smooth function that contains a time lag term and satisfies the following expression, where $\upsilon(t)$ is a continuous function.

$$\begin{cases}\tau(t) \le \tilde{\tau} \\ x(t) = \upsilon(t), t \in \left[t_0 - \tilde{\tau}, t_0\right]\end{cases} \quad (15)$$

Before proposing the fault-tolerant control technique, the assumptions of Eqs. (16)–(19) will be made for the system with state time lags. Where, λ and μ are positive real numbers; P, N, W, and Q are positive definite symmetric matrices.

$$\begin{aligned}&\varphi\left(x(t), x\left(t-\tau(t)\right)\right) = \mathbf{B}\xi\left(x(t), x\left(t-\tau(t)\right)\right) \\ &\left\|\xi\left(x(t), x\left(t-\tau(t)\right)\right)\right\| \le \lambda\left\|x(t)\right\| + \mu\left\|x\left(t-\tau(t)\right)\right\|\end{aligned} \quad (16)$$

$$\mathbf{P}\left(\mathbf{A}+\mathbf{BG}\right) + \left(\mathbf{A}+\mathbf{BG}\right)^T \mathbf{P} = -\mathbf{N}, \mathbf{N} > 0 \quad (17)$$

$$\begin{aligned}&\mathbf{W}\left(\mathbf{A}-\mathbf{EC}\right) + \left(\mathbf{A}-\mathbf{EC}\right)^T \mathbf{W} = -\mathbf{Q}, \mathbf{Q} > 0 \\ &\mathbf{B}^T\mathbf{W} = \mathbf{C}\end{aligned} \quad (18)$$

$$\mathbf{F}_a = \mathbf{B}\mathbf{R}^T \quad (19)$$

Based on a mathematical model of system dynamics with a time lag, this study will design an adaptive observer. Fig. 2 represents the observer and fault-tolerant control diagram of the system [17].

Eq. (15) is the functional expression of the adaptive observer, where $\hat{x}$ represents the estimated values of the state vector, and $\hat{f}_a$ represents the estimated values of the fault vector. ρ denotes the adaptive parameters.

$$\begin{cases}\dot{\hat{x}}(t)=\mathbf{A}\hat{x}(t)+\mathbf{B}u(t)+1/2\mathbf{B}\hat{\rho}(t)y(t)-\hat{y}(t)+F_a\hat{f}_a(t)\\ \hat{y}(t)=\mathbf{C}\hat{x}(t)\end{cases} \tag{20}$$

The following functional expressions serve as representations of the fault adaptive law and the parameter adaptive law. Where ζ and η denote positive real numbers and positive definite symmetric matrices, respectively.

$$\begin{aligned}\dot{\hat{\rho}}(t)&=\zeta\left\|y(t)-\hat{y}(t)\right\|^2\\ \dot{\hat{f}}_a(t)&=\eta R\left(y(t)-\hat{y}(t)\right)\end{aligned} \tag{21}$$

In this study, a closed-loop control system for the output FFT of a steam hydroturbine regulating system is created. It consists of an adaptive compensator $u_s(t)$ and a fault-tolerant controller $u_f(t)$. The expression of the output FFT is as follows, and the pseudo-inverse matrix of B is denoted by B^+.

$$\begin{aligned}&u(t)=u_s(t)+u_f(t)\\ &\begin{cases}u_s(t)=\mathbf{G}\hat{x}(t)-1/2\hat{\rho}(t)\left(y(t)-\hat{y}(t)\right)\\ u_f(t)=-\mathbf{B}^+F_a\hat{f}_a\end{cases}\end{aligned} \tag{22}$$

By integrating the mathematical model of the system dynamics with the state time lag and its associated assumptions, it is possible to show that the closed-loop control system is almost in a global steady state.

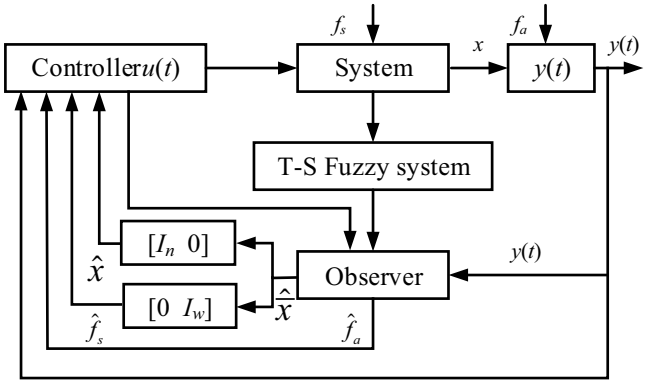

Fig. 2. System fault-tolerant control and fault observation.

3.2. Design of fault-tolerant control parameters with state time lag

The actuator of the hydroturbine regulation system has a significant inertia time constant, making it impossible for the traditional water guide system to provide real-time tracking regulation control under load variation [18]. To lessen the impact of state time delay, the delay time effects of hydraulic relay displacement and actuator fault parameters are introduced in this study. Under the influence of rigid water hammer, the FFT control model developed in Section 3.1 is validated. Four fault-tolerant controllers are designed in the system, which are respectively represented as u_1, u_2, u_3, u_4. Eq. (23) is the dynamic mathematical model and parameters of the design [19].

$$\begin{cases}\dot{\delta}=\omega_0\omega+u_1\\ \dot{\omega}=\dfrac{1}{T_{ab}}\left[m_t-\dfrac{E'_qV_s}{x'_{d\Sigma}}\sin\delta-\dfrac{V_s^2}{2}\dfrac{x'_{d\Sigma}-x_{q\Sigma}}{x'_{d\Sigma}x_{q\Sigma}}\sin 2\delta-D\omega\right]+u_2\\ \dot{m}_t=\dfrac{1}{T_{ab}}\left[-m_t+e_y y\left(t-\tau(t)\right)-\dfrac{ee_yT_w}{T_y}\left(u_4-y\left(t-\tau(t)\right)\right)\right]+u_3\\ \dot{y}=\dfrac{1}{T_y}\left[u_4-y\left(t-\tau(t)\right)\right]\end{cases} \tag{23}$$

where ω indicates the relative deviation of generator speed, δ indicates the relative deviation of generator power angle. Other control parameters and their values are shown in Table 2.

For the dynamic mathematical model with time lag shown in Equation (14), the coefficient matrices are taken as: $\mathbf{A}=\begin{bmatrix}0&314&0&0\\0&-0.0625&0.125&0\\0&0&-1.333&0\\0&0&0&0\end{bmatrix}$, $\mathbf{B}=\mathbf{F}_a=\begin{bmatrix}1&0&0&0\\0&1&0&0\\0&0&1&-14\\0&0&0&10\end{bmatrix}$, $\mathbf{R}=\mathbf{W}=\begin{bmatrix}1&0&0&0\\0&1&0&0\\0&0&1&0\\0&0&0&1\end{bmatrix}$.

Table 2
Design of output FFT parameters

Test parameters	Parameter name	Parameter values	Test parameters	Name	Parameter values
D	Damping factor	0.5 p.u.	e	Intermediate variables of the receiver	0.7 p.u.
e_y	Stroke transfer coefficient	1.0 p.u.	e_{qh}	Head transfer coefficient	0.5 p.u.
T_{ab}	Mechanical inertia time constant	8.0 s	T_y	Reaction time constant of the receiver	0.1 s
E'_q	transient potential	1.35 p.u.	ω_0	Rated angular speed of the generator	314 rad/s
V_s	Infinite bus voltage	1.0 p.u.	T_w	/	1.5 s
$x'_{d\Sigma}$	/	1.15 p.u.	$x_{q\Sigma}$	/	1.5 p.u.

Assuming the state time lag $\tau(t) = 0.5\cos(t)$, the function $\phi(\cdot)$ with the state time lag term has the following relationship.

$$\varphi\left(x, x\left(t-\tau\left(t\right)\right)\right)=\begin{bmatrix}-0.1467\sin\left(\delta\right)+0.01195\sin\left(2\delta\right)\\ 15.333y\left(t-0.5\cos\left(t\right)\right)\\ -10y\left(t-0.5\cos\left(t\right)\right)\end{bmatrix} \tag{24}$$

Let the parameter $k = 0.5$, the positive definite symmetric matrix $\eta=\begin{bmatrix}50&0&0&0\\0&100&0&0\\0&0&100&0\\0&0&0&50\end{bmatrix}$. Based on the assumptions in Eq. (17), the matrices P, N, and G are taken as follows.

$$\mathbf{N}=\begin{bmatrix}1&0&0&0\\0&1&0&0\\0&0&1&0\\0&0&0&1\end{bmatrix}$$

$$\mathbf{P}=\begin{bmatrix}0.1051&0.0085&0.0429&0.0375\\0.0085&0.0503&-0.0061&0.0098\\0.0429&-0.0061&0.0956&0.0236\\0.0375&0.0098&0.0236&0.0734\end{bmatrix}$$

$$\mathbf{G}=\begin{bmatrix}-6.0352&-319.7639&9.7923&-0.2500\\4.7441&-9.7403&-9.3181&-3.6930\\3.9465&14.5910&-19.0684&-4.3376\\0.3319&0.7160&-0.8843&-0.8730\end{bmatrix}$$

Eq. (25) is the fault vector function under the optimal fault-tolerant control technique.

$$f_a\left(t\right)=\begin{cases}0, & t<5s & \text{Trouble - free}\\ f_1, & 5\le t<10s & \text{Constant value trouble}\\ f_2, & 10\le t\le 20s & \text{Time - varying trouble}\end{cases} \tag{25}$$

And $f_1=\begin{bmatrix}f_{a1}\\f_{a2}\\f_{a3}\\f_{a4}\end{bmatrix}=\begin{bmatrix}5\\-5\\4\\-4\end{bmatrix}, f_2=\begin{bmatrix}f_{a1}\\f_{a2}\\f_{a3}\\f_{a4}\end{bmatrix}=\begin{bmatrix}2\\0.5\cos\left(t\right)\\3\\0.5\cos\left(t\right)\end{bmatrix}$.

Based on the above selected control parameters, the computational expression of the fault-tolerant controller can be obtained as shown in Eq. (26) [20].

$$\begin{bmatrix}u_1\\u_2\\u_3\\u_4\end{bmatrix}=\begin{bmatrix}u_\delta\\u_\omega\\u_{m_t}\\u_y\end{bmatrix}=\begin{bmatrix}-6.0352&-319.7639&9.7923&-0.2500\\4.7441&-9.7403&-9.3181&-3.6930\\3.9465&14.5910&-19.0684&-4.3376\\0.3319&0.7160&-0.8843&-0.8730\end{bmatrix}\begin{bmatrix}\hat{\delta}\\\hat{\omega}\\\hat{m}_t\\\hat{y}\end{bmatrix}$$
$$+\cdots-\frac{1}{2}C\hat{\rho}t\begin{bmatrix}\delta-\hat{\delta}\\\omega-\hat{\omega}\\m_t-\hat{m}_t\\y-\hat{y}\end{bmatrix}-B^+\begin{bmatrix}1&0&0&0\\0&1&0&0\\0&0&1&-14\\0&0&0&10\end{bmatrix}\begin{bmatrix}\hat{f}_{a1}\\\hat{f}_{a2}\\f_{a3}\\f_{a4}\end{bmatrix} \tag{26}$$

4. Hydroturbine regulation system fault diagnosis and control simulation test

4.1. Simulation test for online predictive diagnosis of hydroturbine regulation system faults

Numerical simulations are performed to test the predictive control effect designed by the study, using the operating parameters of an actual hydropower plant as an example. The initial values of the system state is $[x_1,x_2,x_3,\delta,\omega,y]^T = [0.01,0.01,0.01,0.01,0.01,0.01]^T$, the control time domain $L = 1$, the prediction time domain $P = 10$, and the sampling period $T = 0.02$s. δ indicates the generator power angle, ω indicates the generator angular velocity, and y indicates the guide vane opening. The steady state parameters in the absence of disturbances is $Y_s = [\delta,\omega,y]^T = [1.5,0.1,0.8]^T$. Fig. 3 shows the output response curves, where Fig. 3a–c represent the constant-value perturbations of $d = 0.1$, $d = 0.03$, and $d = 0.1$ added between $10s \le t \le 12s$, respectively.

From the output response curves in Fig. 3, it can be seen that the state feedback predictive control based on the T-S fuzzy model has a better control effect. In the case of no disturbance, the power angle δ, angular velocity ω and guide vane opening y of the generator reach the steady state around 3.0s, with short response time and small overshoot of the curves. When the constant disturbance was added at the 10th seconds of system operation, the output response curve appeared jittering and stabilized quickly within 1 s. When the constant disturbance was removed at the 12th seconds of system operation, the output response curve showed reverse oscillation and returned to the stable state within 1 s. From this result, it can be inferred from the results that when the hydroturbine regulation system is subjected to external random disturbance, the output response curve will appear long time low frequency oscillation. However, the predictive controller can reduce the vibration amplitude of the generator power angle, so as to ensure the rapid stabilization and reduce the out-of-step phenomenon.

To test the state tracking effect of the predictive controller, three different experimental parameters are set to test the tracking effect of the system. With in the range of [0,8],[8,14],[14,20], set $Y_s = [\delta,\omega,y]^T$ to $[1.5,0.1,0.8]^T$, $[1.7,0.12,1.0]^T$, and $[1.3,0.08,0.6]^T$, respectively. Fig. 4 shows the state tracking response curves, where Fig. 4a–c represent the power angle δ, angular velocity ω, and guide vane opening y of the generator, respectively.

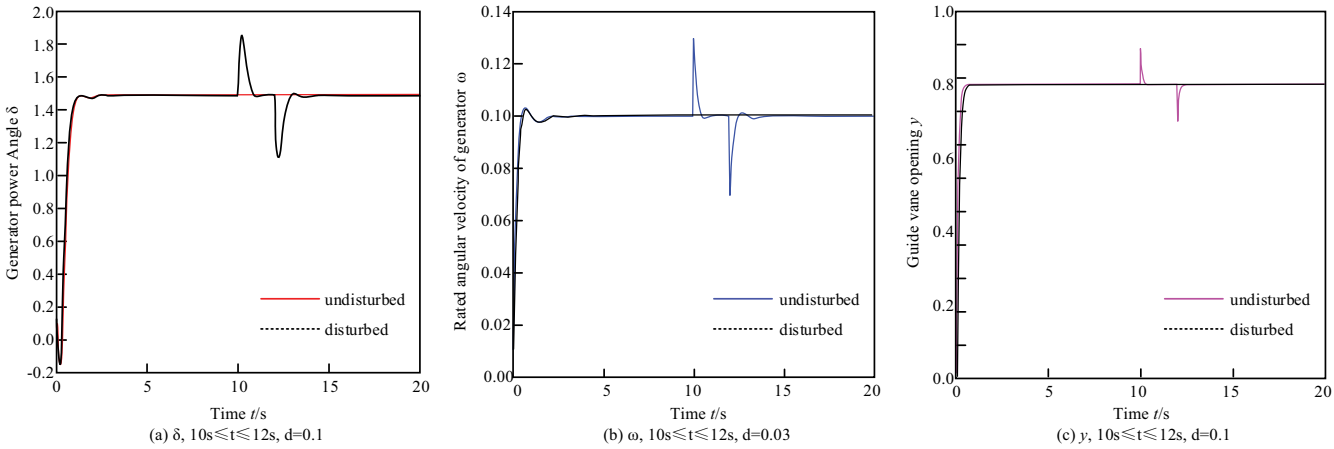

Fig. 3. Output response curve. (a) δ, 10s ≤ t ≤ 12s, d = 0.1, (b) ω, 10s ≤ t ≤ 12s, d = 0.03 and (c) y, 10s ≤ t ≤ 12s, d = 0.1.

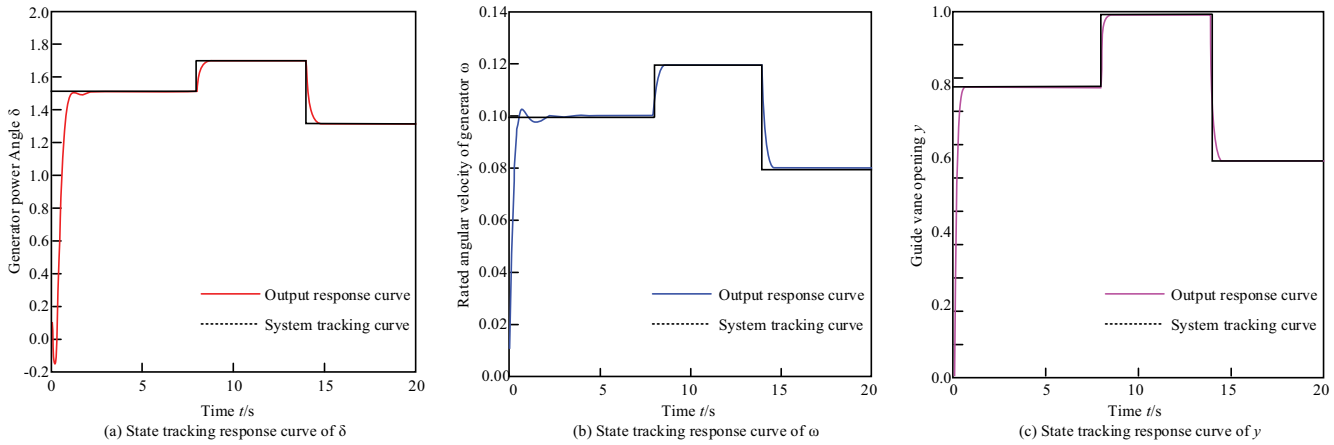

Fig. 4. State tracking response curve of (a) δ, (b) ω and (c) y.

The steady state is interrupted during the 8th and 14th seconds of the system's operation, at which point the state feedback predictive controller kicks in and the system is promptly adapted to the new steady state. From the tracking response curve in Fig. 4, it can be seen that the system is in the regulation phase for a shorter time and the overshoot is small, which indicates that the state feedback predictive controller has a better control effect. The predictive controller suggested in this study cannot only speed up the restoration of the system's steady state under interference, but it can also lower the system's energy consumption during state transitions.

4.2. Hydroturbine regulation system output FFT simulation test

For the output FFT technique, the setup parameters selected for this study is $x = [\delta,\omega,m_t,y]^T$ and the initial values of the simulation is $\hat{x}(0)=\begin{bmatrix}0 & 0 & 0 & 0\end{bmatrix}^T$, $x(0)$ = [0.1 0.2 0.6 0.3]^T. From Fig. 5, the state response curves where Fig. 5a–d represent the relative deviation of power angle, relative deviation of angular velocity, relative deviation of output power, and relative deviation of guide vane opening, respectively.

When 5s ≤ t ≤ 10s, constant faults are used to denote actuator deviation faults, and they usually come from mechanical friction or external disturbances of the system. The findings of the state response in Fig. 5 demonstrate that the system swiftly stabilizes again within 2 s even in the face of constant-value faults or state time lags, which is crucial for the system's regular operation. When 10s ≤ t ≤ 20s, time-varying faults are used to describe the equal-amplitude periodic vibrations, and they usually come from the rotational speed or the main servo motor. As can be seen from the curve states in Fig. 5, the regulated system can still be stabilized quickly. However, there are relatively more fluctuations in the state response curves for time-varying faults and a larger amount of overshoot. This result reflects the effectiveness of the fault-tolerant controller, but there is still room to improve its control accuracy. With different steady state parameters set at 0s ≤ t ≤ 5s, 5s ≤ t ≤ 10s, and 10s ≤ t ≤ 20s, Fig. 6 shows the tracking response curves to mechanical and time-varying faults, where Fig. 6a–d represent the power angle fault, angular velocity fault, output power fault, and guide vane opening fault, respectively.

From Fig. 6, it can be seen that the system oscillates at the 5th second and 10th second. However, after that, the response curve quickly reaches the steady state and the

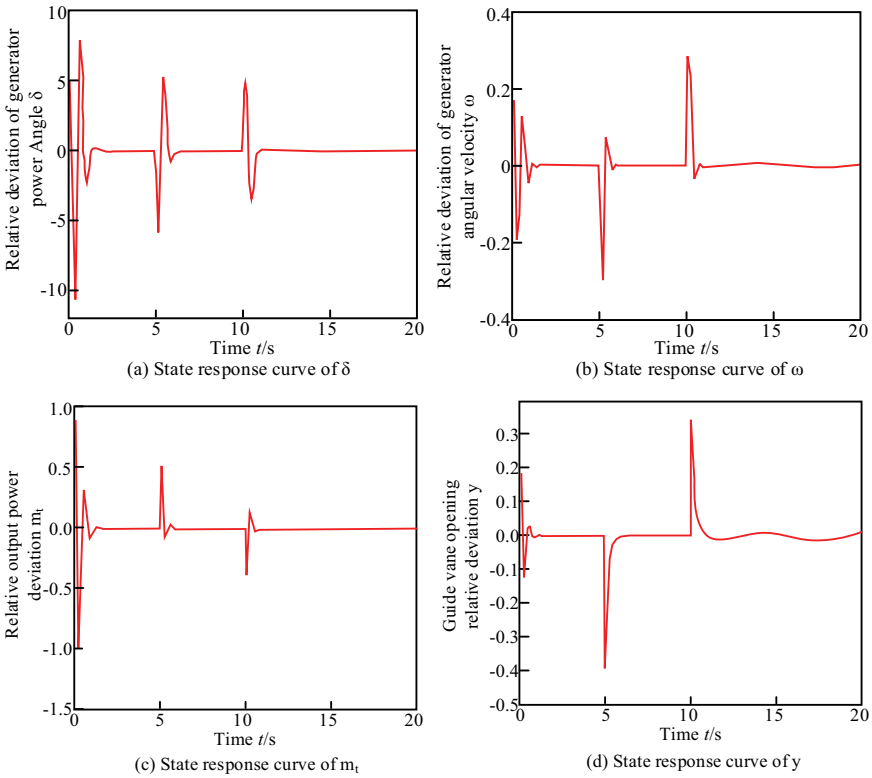

Fig. 5. State response curve of (a) δ, (b) ω, (c) m_t and (d) y.

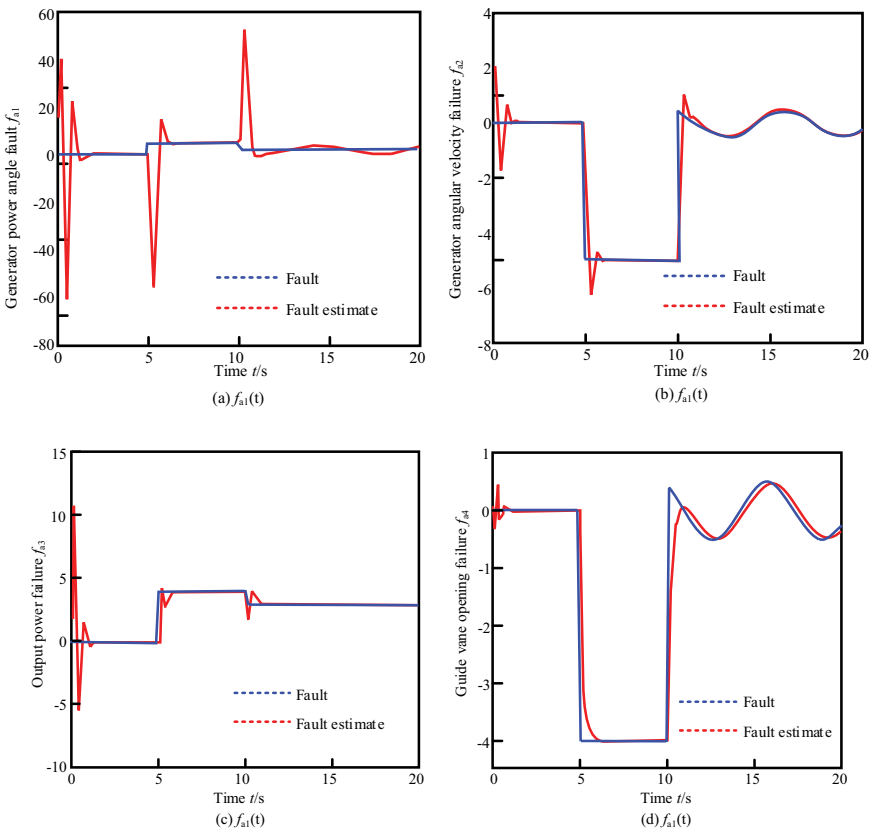

Fig. 6. Fault tracking response curve. (a) $f_{a1}(t)$, (b) $f_{a1}(t)$, (c) $f_{a1}(t)$ and (d) $f_{a1}(t)$.

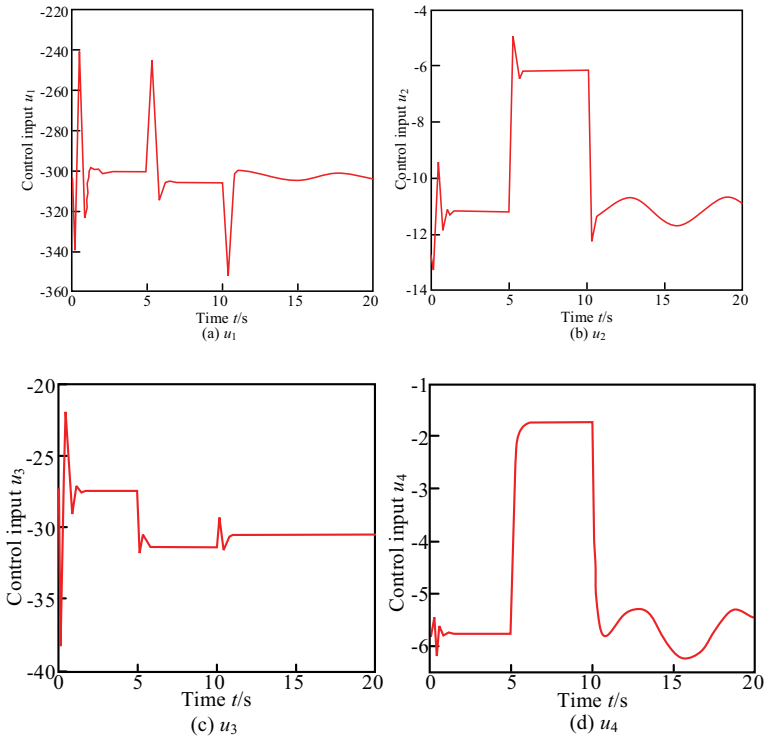

Fig. 7. Control input curve of the system controller: (a) u_1, (b) u_2, (c) u_3 and (d) u_4.

system overshoot is small, which indicates that the adaptive observer shows good recognition and tracking effect on the mechanical faults of the system. It is assumed that the adaptive observer can quickly identify and track the mechanical faults or time-varying faults when they occur in the system, and provide real-time feedback to the fault-tolerant controller online to ensure the control effect. Fig. 7 shows the input curves of the output FFT system, where Fig. 7a–d represent the controllers u_1, u_2, u_3, and u_4, respectively. Fig. 7 is compared and analyzed with Fig. 6 as a way to observe the feedback effect of the controller on system faults.

As can be seen from the control input curves in Fig. 7, all four controllers show curve changes at 5s ≤ t ≤ 10s and 10s ≤ t ≤ 20s, and there is a relationship between the curve trends and the response curve to system faults. This indicates that the fault-tolerant controller responds when a fault occurs in the system, which provides a faster response time for the regulation system and reduces the fault fluctuation of the system. The adaptive observer can keep an online eye on the operation of the system in real-world engineering applications. The system fault fluctuation can be stabilized and the effectiveness of hydroturbine operation and maintenance can be increased by quickly recognizing and analyzing system faults.

5. Conclusion

The conventional hydroturbine regulation system is unable to provide timely feedback in the face of random mechanical failures or time-varying faults, which will lead to control system failure. This paper focuses on output FFT approaches with state time lag and system failure diagnostics, and it numerically simulates and tests these techniques using real-world operating conditions. The findings demonstrate that the T-S fuzzy model-based predictive control system has high tracking control effect and can swiftly settle with a modest overshoot in the presence of external disturbances within 1 s. The fault tolerant controller can also maintain system stability in less than 2 s. It provides effective input, monitoring, and a calming impact when a system fails, which indicates that the fault-tolerant controller proposed in the research has good applicability. Although the hydroturbine regulation system controller designed in this research has shown good control capability, there is still room for improvement in its control accuracy, which will be further developed in the future research.

Acknowledgement

This paper is funded by the National Key Research and Development Program of China “Cooperative study on comprehensive evaluation methods of wave and tidal currents energy technology” (2019YFE0102500).

References

[1] T. Hosotani, T. Shigemitsu, Y. Kawaguchi, T. Ikebuchi, Study on high pressure design of contra-rotating small hydroturbine, Int. J. Fluid Mach. Syst., 12 (2019) 268–276.
[2] H.-J. Noh, J.-S. Lee, Y.-J. Kim, Micro-energy harvesting based on vortex-induced vibration of cross-flow hydroturbine with various cantilever beam configurations, IOP Conf. Ser.: Earth Environ. Sci., 240 (2019) 022034, doi: 10.1088/1755-1315/240/2/022034.

[3] C.M. Shashikumar, R. Honnasiddaiah, V. Hindasageri, V. Madav, Studies on application of vertical axis hydro turbine for sustainable power generation in irrigation channels with different bed slopes, Renewable Energy, 163 (2021) 845–857.
[4] C. Wang, D. Wang, J. Zhang, Experimental study on isolated operation of hydro-turbine governing system of Lunzua hydropower station in Zambia, Renewable Energy, 180 (2021) 1237–1247.
[5] H. Li, H. Diaz, C. Guedes Soares, A developed failure mode and effect analysis for floating offshore wind turbine support structures, Renewable Energy, 164 (2021) 133–145.
[6] J. Zhang, F. Yang, C. Liang, Y. Zhang, Y. Li, An SVDD-based post-processing approach for vibration risk assessment of the hydro-turbine-generator in a large hydropower station, J. Low Freq. Noise Vibr. Act. Control, 40 (2021) 1309–1334.
[7] Y. Chen, F. Tong, Stability analysis of hydro-turbine governing system based on machine learning, Chin. Phys. B, 30 (2021) 336–343.
[8] J. Zhang, B. Xu, D. Chen, H. Li, Md A. Mahmud, W. Govaerts, Numerical bifurcation and continuation of a nonlinear hydro-turbine governing system in a single-machine infinite-bus power system, IET Gener. Transm. Distrib., 14 (2020) 3346–3355.
[9] P. Guo, H. Zhang, D. Gou, Dynamic characteristics of a hydro-turbine governing system considering draft tube pressure pulsation, IET Renewable Power Gener., 14 (2020) 1210–1218.
[10] D. Nan, T, Shigemitsu, T. Ikebuchi, T. Ishiguro, T. Hosotani, Pressure fluctuation on casing wall and investigation to tip leakage flow of contra-rotating small hydro-turbine, Proc. Inst. Mech. Eng., Part A: J. Power Energy, 236 (2022) 506–518.
[11] A. Babu, G. Perumal, H.S. Arora, H.S. Grewal, Enhanced slurry and cavitation erosion resistance of deep cryogenically treated thermal spray coatings for hydroturbine applications, Renewable Energy, 180 (2021) 1044–1055.
[12] B. Xu, X. Luo, M. Egusquiza, W. Ye, J. Liu, E. Egusquiza, D. Chen, P. Guo, Nonlinear modal interaction analysis and vibration characteristics of a Francis hydro-turbine generator unit, Renewable Energy, 168 (2021) 854–864.
[13] K. Rajagopal, H. Jahanshahi, S. Jafari, R. Weldegiorgis, A. Karthikeyan, P. Duraisamy, Coexisting attractors in a fractional order hydro turbine governing system and fuzzy PID based chaos control, Asian J. Control, 23 (2021) 894–907.
[14] S. Kesharwani, K. Tripura, P. Singh, Classical hydraulic ram pump performance in comparison with modern hydro-turbine pumps for low drive heads, Proc. Inst. Mech. Eng., Part A: J. Power Energy, 235 (2021) 1463–1486.
[15] E. Gallego, A. Rubio-Clemente, J. Pineda, L. Velásquez, E. Chica, Experimental analysis on the performance of a pico-hydro Turgo turbine, J. King Saud Univ., 33 (2020) 266–275.
[16] R. Kumari, K.K. Prabhakaran, K. Desingu, T.R. Chelliah, S.V. Appa Sarma, Improved hydroturbine control and future prospects of variable speed hydropower plant, IEEE Trans. Ind. Appl., 57 (2020) 941–952.
[17] U. Shrestha, Z. Chen, Y.D. Choi, Correlation of the sediment properties and erosion in Francis hydro turbine runner, Int. J. Fluid Mach. Syst., 12 (2019) 109–118.
[18] D. Zhou, J. Gui, Z.D. Deng, H. Chen, Y. Yu, A. Yu, C. Yang, Development of an ultra-low head siphon hydro turbine using computational fluid dynamics, Energy, 181 (2019) 43–50.
[19] B. Xu, H.-B. Jun, D. Chen, H. Li, J. Zhang, C.J.C. Blanco, H. Shen, Stability analysis of a hydro-turbine governing system considering inner energy losses, Renewable Energy, 134 (2019) 258–266.
[20] K. Song, W.-Q. Wang, Y. Yan ,Numerical and experimental analysis of a diffuser-augmented micro-hydro turbine, Ocean Eng., 171 (2019) 590–602.